6. Analysis

6.1. Electron-Positron Pair Selection.

1. The event passes the e+e- hardware trigger and PRUDE filter, and is written to a disk file.

2. A subset of this file passing loose cuts called a DST (Data Summary Tape) is created.

3. A Fortran program reconstructs CCAL elements into clusters. Each cluster pair is a potential e+e- candidate.

4. At most one cluster pair from the event is selected as an e+e- candidate. An n-tuple, a file accessed by the PAW analysis package (Physics Analysis Workstation), stores kinematic variables for each pair.

5. Within PAW, cuts are made on the candidate event's acoplanarity, akinematics, number of on-time clusters, total energy, and the invariant mass.

6. Events passing step 5 fill an histogram: The cosine of the polar angle in the center-of-mass frame for each electron, as determined by the scintillating fiber detector.

7. The angular distribution from step 6 is fit to the function $A + B* \cos^2(*)$. The angular distribution parameter is B/A.
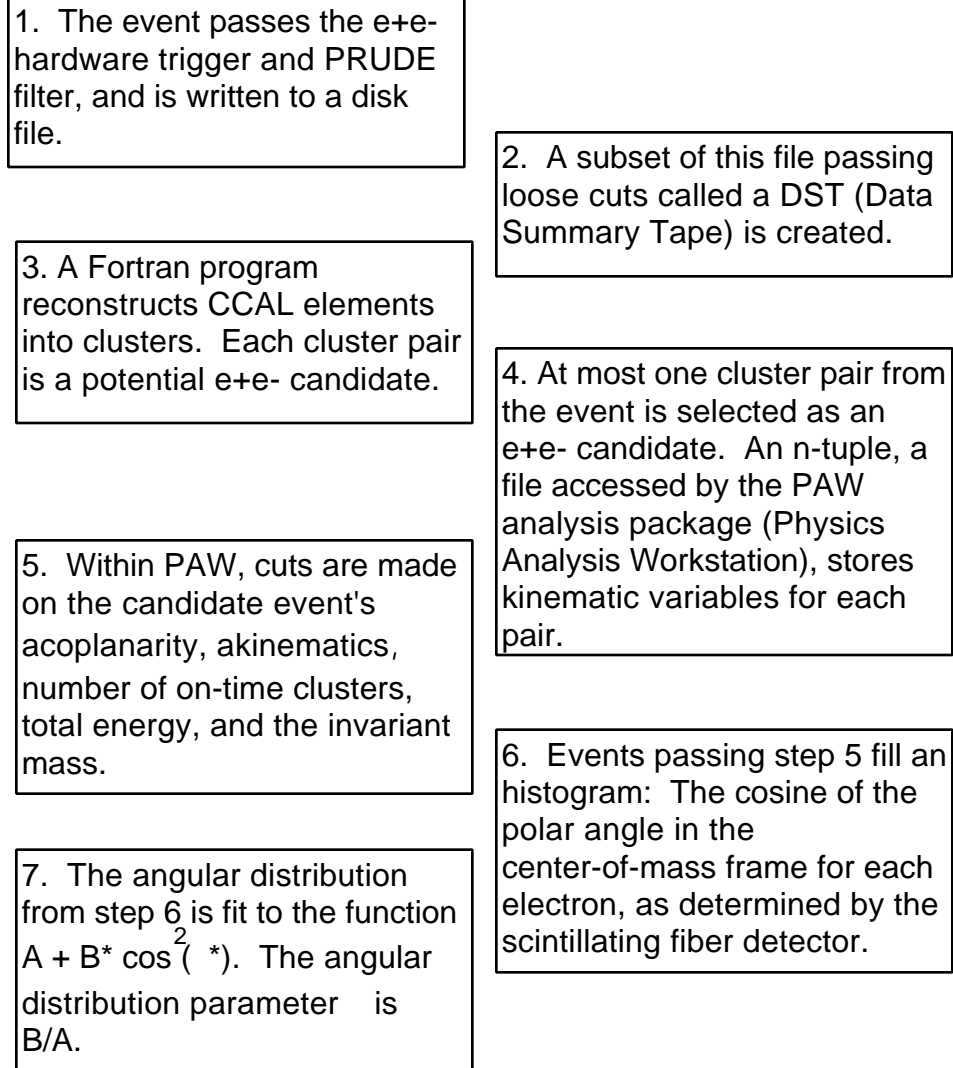
Figure 6.1 : Data Analysis Flow Chart.

The sequence of selections on electron-positron candidate events is shown schematically in Figure 6.1. Initially (Step 1, Figure 6.1), events that pass the hardware e^+e^- trigger are reconstructed by the PRUDE filter and written

to disk. From these resident disk files, loose cuts are applied (Step 2, Figure 6.1) in order to produce a DST file (Data Summary Tape), also residing on disk. A DST contains a subset of all the events in the disk file that do not include the large hadronic background present below 2.7 GeV. The event is rejected if (a) the event did not fire Gatemaster bit 1 (the e^+e^- trigger), (b) the number of clusters seen by the central calorimeter is greater than 20, or (c) the largest possible invariant pair mass (on-time or out-of-time) constructed from a cluster pair is less than 2.7 GeV, as determined from the energy deposits and angles given by the central calorimeter.   All possible combinations of cluster pairs are considered, except when one of the clusters (a) is not on-time with respect to the e^+e^- trigger, or (b) does not exceed a minimum cluster energy of 200 MeV .

When a particle such as an electron enters the CCAL, it creates an electromagnetic shower which produces Cerenkov light in several neighboring lead glass blocks.   The amount of Cerenkov light is proportional to the amount of energy deposited in each block.   A software program called the clusterizer searches for possible "seed" blocks, around which the energy deposits are grouped into clusters (Step 3, Figure 6.1). A cluster is the CCAL's representation of the particle that entered it. For this analysis, cluster thresholds were set at 5 MeV for the seed block of the cluster, and 20 MeV for the surrounding 3-by-3 grid. A cluster pair is defined to be "on-time" if the TDC values (which flag the cluster creation with respect to the time the interaction occurred) of its largest energy deposits are on-time.

From the smaller DST file, further cuts are applied to the data to establish the thesis sample (Step 4, Figure 6.1) and event information is written to an n-tuple, a file that stores processed information for future use within PAW (the Physics Analysis Workstation analysis package). A typical n-tuple may hold the values of 35 to 50 kinematic variables per event. If an on-time cluster pair generates an invariant mass closest to the resonance in question, and said invariant mass is greater than 2.7 GeV, then that cluster pair is chosen to be the e^+e^- candidate from the event. There is no way to tell in this experiment which cluster is the positron and which is the electron.

At this juncture the thesis sample is refined using the PAW analysis package (Step 5, Figure 6.1). Many different analysis cuts, like those discussed later in Section 6.3 to determine the thesis sample, can be made. For example, suppose one wants to plot the invariant mass of all the events in the n-tuple with only 2 on-time clusters. Kumac files may include a large list of commands like those below, and allow Fortran programs to be called from within PAW to analyze the data. The general procedure is as follows:

```
> pawX11                                ! Launch the PAW software
                                        ! package.
>hi/file 1 /scratchj/mctaggar/jpsi.ntp  ! Load the desired n-tuple.
```

```
>ntuple/plot 20.s12 ontime.eq.2          ! Display an histogram of the

                                         ! invariant mass (s12) of all

                                         ! events  whose value

                                         ! of "ontime" is 2.
```

After the final thesis sample has been ascertained, one may plot the angular distribution in an histogram (Step 6, Figure 6.1), and fit this histogram to obtain the angular distribution parameter   (Step 7, Figure 6.1). The details of the fit will be presented in Chapter 7: The remainder of Chapter 6 focuses on the selection of the thesis sample. Section 6.2 determines which polar angle information is included in the angular distribution histogram. In Section 6.3 the analysis cuts are fully detailed, and finally in Sections 6.4 and 6.5 any background contamination remaining in the sample and possible bias with the hardware trigger are discussed respectively.

6.2. Polar Angle from Fibers and CCAL.

In the experiment there are several ways to define the polar angles of the e^+e^- pair. Primarily one may use either the information given by the scintillating fiber tracker,[92] that given by the central calorimeter, or some combination of the two. The CCAL has the advantage of yielding the particle's energy, azimuth and polar angle in the lab. In fact the e^+e^- pair is chosen with these 3 variables

and whether the CCAL clusters are on-time. However, due to the finer resolution of the fibers and the behavior of the CCAL clusterizer, the angle that is included in the final angular distribution comes from the scintillating fibers associated with the CCAL cluster and not directly from the CCAL cluster itself. Furthermore, no combination of the two angles are attempted either.

In reconstructing final e^+e^- states, the present offline clusterizer has a preference for centering clusters across the face of a calorimeter block: Away from block centers and toward the block edges. This does not result in a smooth angular distribution of the e^+e^- in cos(*). The primary reason for this behavior is that the resolution of the calorimeter is better near the edges of the blocks (where 2 photomultiplier tubes can see the event) than at the center (where only one will receive the energy deposit).

The clusterizer is also better equipped to handle the 2 photon decays of resonances like the $_2$ or the $_c$ than the e^+e^- decays studied here. Its algorithms search for energy deposits to group into clusters, and along with the e^+e^- in the event may come delta rays from the interaction of the electrons with the detectors. The position of the cluster can be affected by these delta rays that get absorbed in the clusterizing process.

The result is an unnaturally high chi-square per degree of freedom for the

angular distribution, which is not related to whether both electrons are contained within the geometrical acceptance of the CCAL. This oscillation of CCAL angular distributions about the fit curve, which repeats after every CCAL block, is easily seen in Figure 6.2. Using only the CCAL information, the chi-square per degree of freedom for the final angular distribution of this thesis would be over 2.0 (the nominal value is 1.0 per degree of freedom).

The CCAL shower Monte Carlo[93] for e835 attempts to describe the general behavior of the lead-glass calorimeter blocks in response to photons and electrons passing through it by integrating over the shower shape instead of producing secondary showering particles as the GEANT version does, but once fully tuned it will deliver a very fast estimation of the response of the calorimeter with many thousands of events. In principle a fully-tuned Monte Carlo (either kind) will correct angular distributions like those found in Figure 6.2 when it can replicate qualities such as acoplanarity, akinematics, where the electron hits a CCAL block across the block face, and bring the chi-square of the final fit to near 1.0 per degree of freedom. However, it was decided for this thesis that the present form of the CCAL shower Monte Carlo and the current set of tuning parameters did not satisfy all of these requirements.
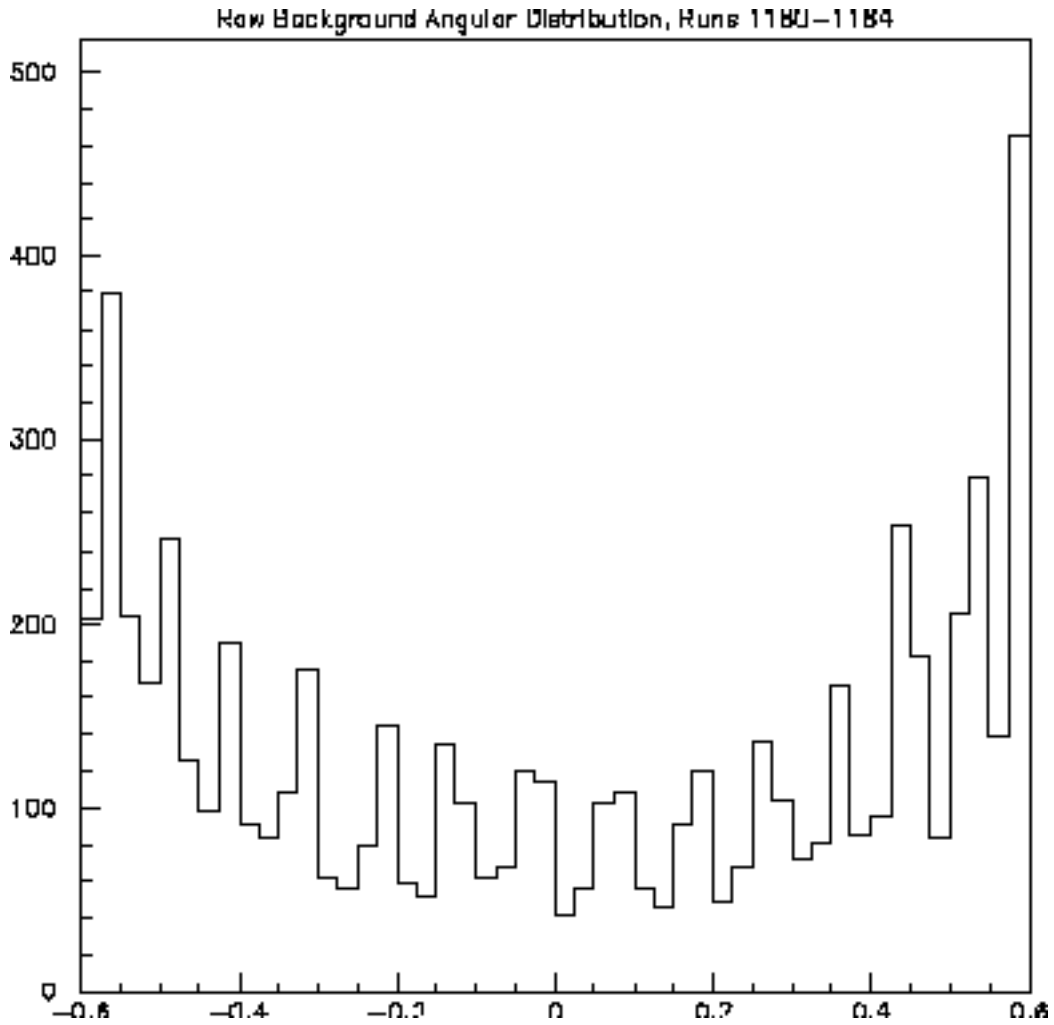
Figure 6.2: Behavior of the CCAL Clusterizer: Raw Angular Distribution
of Background Runs 1180-1184.

Angular distributions using the scintillating fibers do not suffer from this

repetitive behavior seen in the CCAL distributions because the fibers are

physically finer than the face of a CCAL block(~1 mrad [92] vs. ~10 mrad [44]).

However, the fiber angular distribution is not completely independent of the

corresponding CCAL distribution. Fiber hits are associated with particular

CCAL clusters in the process of fitting all the detector elements for charged and neutral tracks. Basically the fiber hits that have the minimum opening angle with respect to a particular CCAL cluster share the same track as that CCAL cluster, but other statistical aspects of the fitting procedure also come into play.

One way to make an independent fiber angular distribution is to choose events that have the minimum akinematics. However, this does not make any demands on the acoplanarity, invariant mass, nor total energy of the event. These are not available from the fibers. Furthermore, the fibers are not 100% efficient: For each e^+e^- pair that passes the analysis cuts (discussed in the next section), there may be 0, 1, or 2 associated fiber tracks. Akinematics from fiber information for a valid e^+e^- pair can only be determined if there are 2 fiber hits per pair.

In this analysis the polar angle is determined from the Z-coordinates of the inner and outer fiber layers. Given the radius of the fiber layer is known, the polar angle in the lab frame can be calculated. If both layers register a hit, the polar angle is taken as the average of the two. Assuming the associated CCAL clusters pass all the analysis cuts, then 0, 1, or 2 entries are made into the histogram for the final angular distribution. This depends upon whether (a) the fiber tracking detector registers and (b) the track is within the fitting region. For the J/ , the fit is applied to the region $-.45 < \cos\left(\theta^*\right) < .45$, which

corresponds in the lab frame to $23.5^\circ < \theta < 57.5^\circ$. For the ψ', the fitting region

is $-.525 < \cos(\theta) < .525$, which corresponds in the lab frame to

$17.3^\circ < \theta < 52.3^\circ$. One result of these choices is that the forward calorimeter is

not used in this analysis, since it lies below 15 degrees. This also removes

background candidates, since the multi-pion channel is forward-peaked.

The efficiency of the scintillating fiber detector for seeing a track is shown

in Figure 6.3. This also includes the geometrical factors shown in Figure 6.4,

and effects like dead channels. Although the efficiency of the fibers affects the

J/ψ angular distribution more, this efficiency is always over 92% for the J/ψ fit,

and over 96% for the ψ' fit.

The effect of selecting the polar angle from the scintillating fiber tracker

instead of the CCAL on the size of the thesis sample is apparent in Table 6.1.

The differences in the event counts (near 1% for both channels) are either due

to migration across the fit boundaries when one chooses the fiber polar angle

over the CCAL polar angle (or vice-versa), a failure to associate a fiber hit to the

correct cluster, or the inefficiency of the fibers. Since both members of the e^+e^-

pair are always contained within the geometry of the detector, and the efficiency

of the scintillating fibers is close to one, no correction by Monte Carlo is made to

the angular distribution of either decay channel.
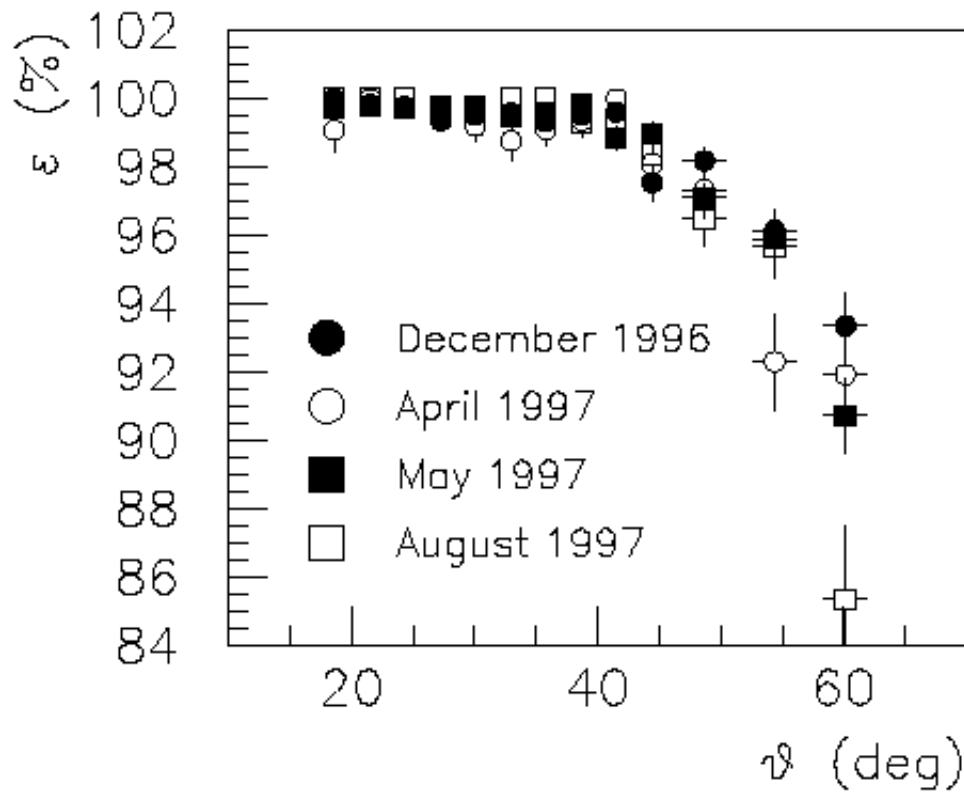
Figure 6.3: Detection efficiency of the scintillating fiber tracker.[92]
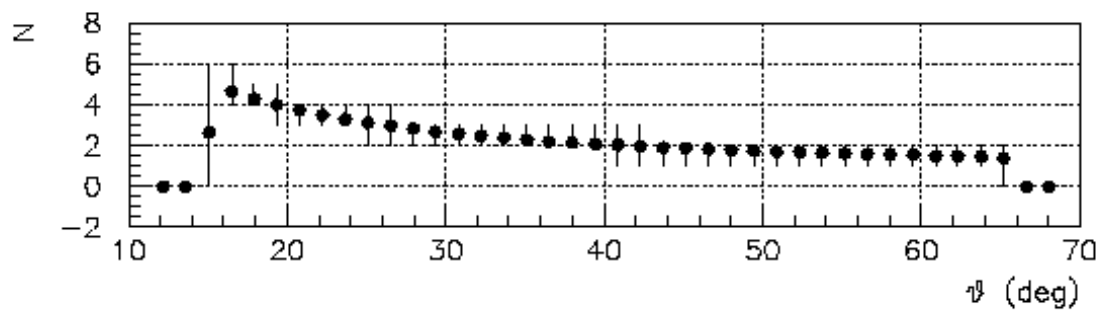

Figure 6.4: Number of fibers hit as a function of polar lab angle.[92]

Run Number	Number of Entries, CCAL	Number of Entries, Scintillating Fiber
908-909	8,244	8,199
3078-3079	2,447	2,419
J/ψ Total	10,691	10,618
877-882	205	207
1006-1018	202	200
1276-1281	532	508
2003-2018	523	524
2218-2253	794	790
3210-3233	461	457
ψ' Total	2,717	2,686

Table 6.1: Number of entries in the final angular distribution when the polar angle is determined from either the CCAL or the scintillating fiber tracker.

Deciding which events contribute to the angular distribution, and therefore to Table 6.1, is the subject of the following section.

6.3. Thesis Sample Selection.

To obtain the angular distribution of the final e^+e^- state, several cuts are applied to the data. The purpose of each cut is to remove events that may simulate an e^+e^- pair decaying from charmonium, but instead arise from the background continuum or multi-pion decays. If the candidate pair from the event passes the following cuts in Table 6.2, and the scintillating fiber tracker

yields a polar angle that falls within the fitting region mentioned in Section 6.2, the event may contribute 0, 1, or 2 entries to the final angular distribution. Otherwise the event is not considered.

1.	2 on-time clusters.
2.	Invariant mass > 2.7 GeV, (J/ψ) Invariant mass > 3.4 GeV, (ψ')
3.	Acoplanarity between -25 milliradians and +25 milliradians.
4.	Akinematics between -25 milliradians and +25 milliradians
5.	4.71 GeV < ETOT < 5.31 GeV (J/ψ) 6.72 GeV < ETOT < 7.62 GeV (ψ')

Table 6.2: Summary of analysis cuts based on CCAL information.

The purpose of this section is to evaluate how the distribution of each of the five variables above is affected by the other cuts, and justify why these cuts were made. However, one should not count the number of events in the following distributions in this section to achieve a final event count, since the fiducial lab angle cuts of Section 6.2 made prior to fitting are not applied to the following plots. As a result the data passing all these cuts will provide at most 2 entries to the angular distribution, but only 1 entry in the following plots. Events

that provide 0 or 1 entries to the angular distribution are still plotted here, and are present when the width of the total energy distribution is determined. Events that fail any of these cuts always contribute zero entries to the angular distribution.

In Appendices A and B the efficiencies of all possible combinations of cuts in Table 6.2 above are listed for each subset of the J/ and the ' data. In this case, fiducial lab angle cuts are performed before calculating the efficiencies of the analysis cuts. The efficiency is defined here as the number of electrons passing all cuts (and included in the fit) divided by the number of electrons achieved by that combination of cuts (and included in the fit). Therefore a set of cuts is 100% efficient if it produces the final data sample. For the ' the efficiencies are generally lower for one or two of the above cuts than similar cuts on the J/ , due to the J/ + decay of the '. Combinations of cuts that include an invariant mass cut of 3.4 GeV have higher efficiencies, since they remove e^+e^- pairs that originate from the J/ .

The first of the analysis cuts is that the event must have only 2 on-time clusters. However, this cut by itself does not prohibit the event from having several out-of-time clusters in addition to these two. Figure 6.5 for the J/ and Figure 6.6 for the ' show how the number of on-time clusters in the sample

90

changes before any cuts are applied and after all other cuts are made. The

extra clusters in the ψ' distribution at the top of Figure 6.6 are due to the (a) the

inclusive decay of the ψ' to the J/ψ, (b) multi-pion decays that accompany

charmonium production, and to a lesser extent (c) the e+e- continuum (i.e.

$p\,\bar{p} \rightarrow e^{+}e^{-}$). Their influence on the study of these exclusive decays of

charmonium are better understood by studying the invariant mass of the

sample. Nevertheless, this particular cut is critical in removing these unwanted

events.
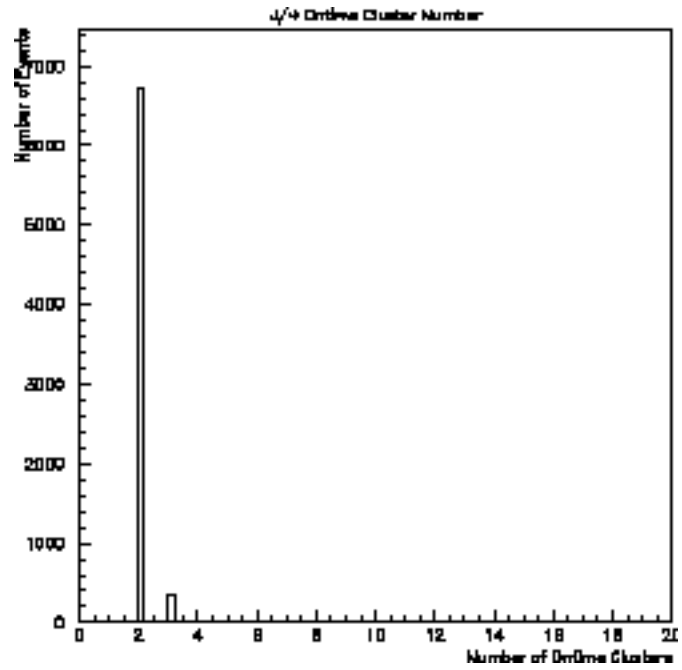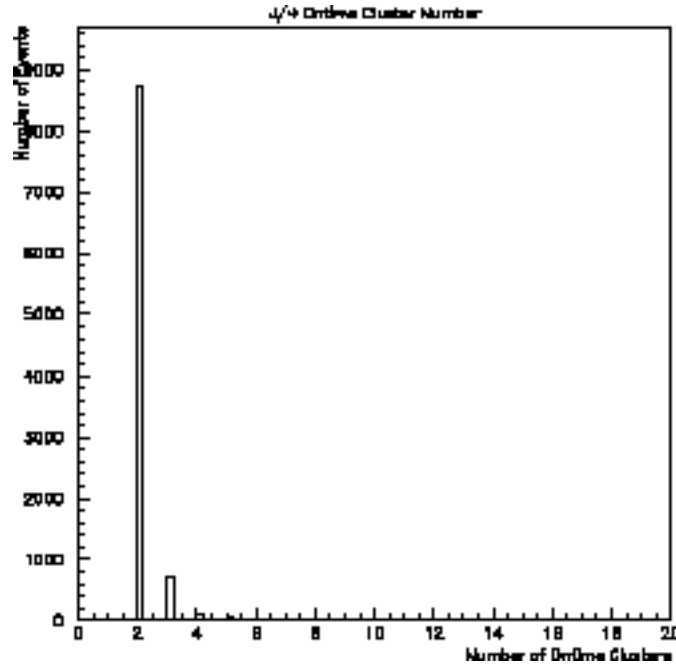
Figure 6.5: J/ψ On-time Cluster Number before any cuts are made (top) and after all other cuts are applied (bottom). Only events with 2 on-time clusters remain in the thesis sample.
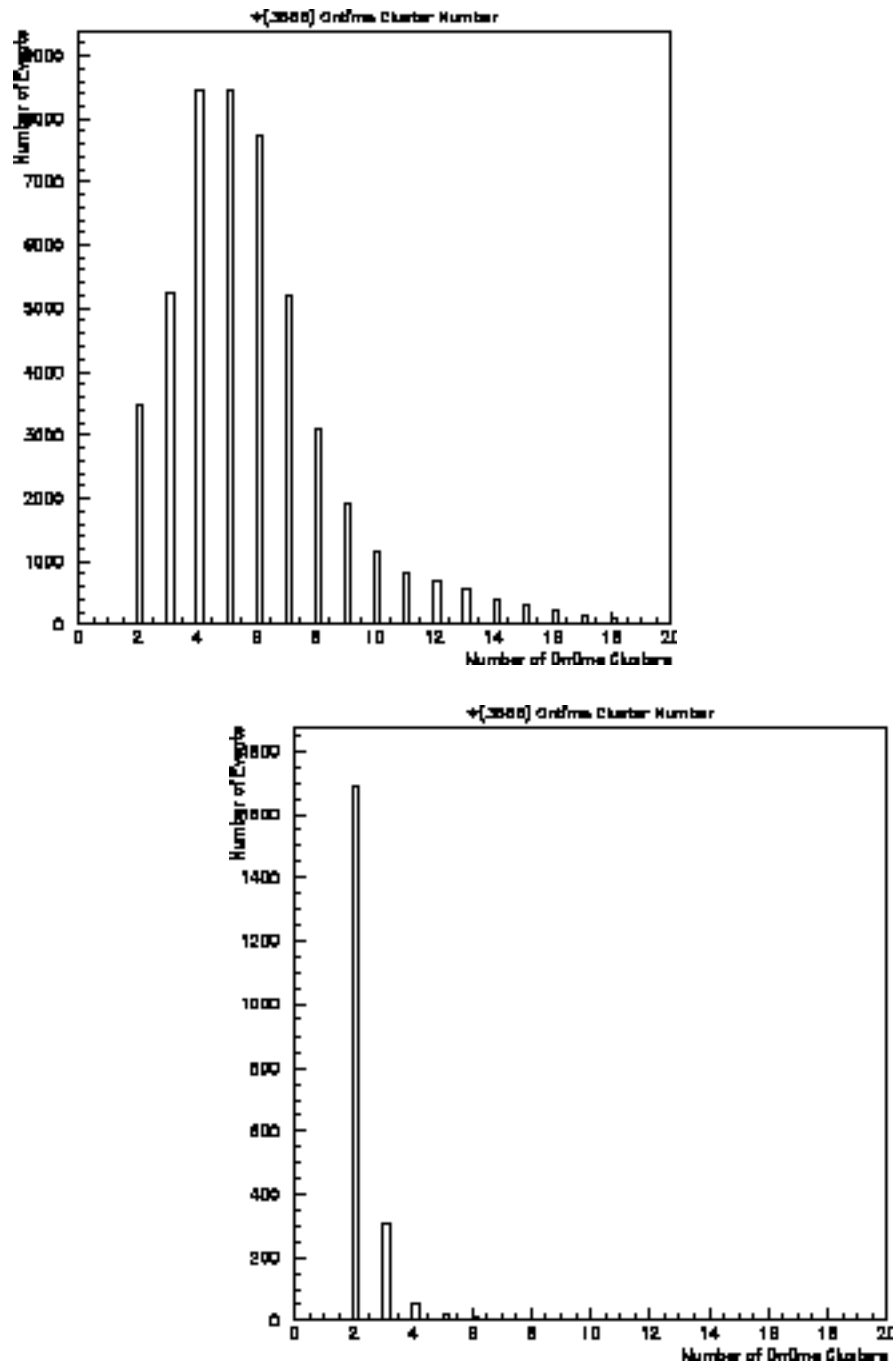
Figure 6.6:　(3686) On-time Cluster Number distributions before any cuts (top) and after all other cuts (bottom) are applied. Only events with 2 on-time clusters remain in the thesis sample.

The invariant mass distributions of the J/ψ are shown in Figure 6.7 before

any cuts are made and after all of the other cuts have been applied. Cluster

pairs included in the final J/ψ sample must have an invariant mass greater than

2.7 GeV. Recall that to be written to the n-tuple, the event must have two

clusters with an invariant mass greater than 2.7 GeV (i.e. neither cluster has to

be on-time). The e^+e^- pair is chosen as the on-time cluster closest to the

resonance in question with respect to the invariant mass, so there are some

e^+e^- pairs with invariant masses less than 2.7 GeV in the n-tuple.

Primarily there are two reasons why the J/ψ exclusive decay is easier to

study than the ψ'. First, the cross-section for producing exclusive decays falls

as $\frac{1}{Q^2}$, so this channel is more prominent at the J/ψ. Also, the resonance below

the J/ψ, the η_c, is not allowed to decay to e^+e^- by parity, so this additional

inclusive channel is not seen in Figure 6.7 as it is in Figure 6.8.

Clearly evident in the top of Figure 6.8 are the two background sources

for the ψ' exclusive decay to an e^+e^- pair before any cuts are made:

Contamination from the multi-pion decays (the large exponential curve), and the

decays of the ψ' to J/ψ + X, where X may be either 2π or simply an η. In the

latter case an e$^+$e$^-$ pair arises from the cascading decay of the J/ψ instead of

the exclusive decay of the ψ', which results in the enhancement around 3.1

GeV.   The exclusive channel remains under the Gaussian centered near 3.6

GeV. At the bottom of Figure 6.8 an invariant mass cut of 3.4 GeV assures that

these two sources have little impact on the exclusive decay channel. The

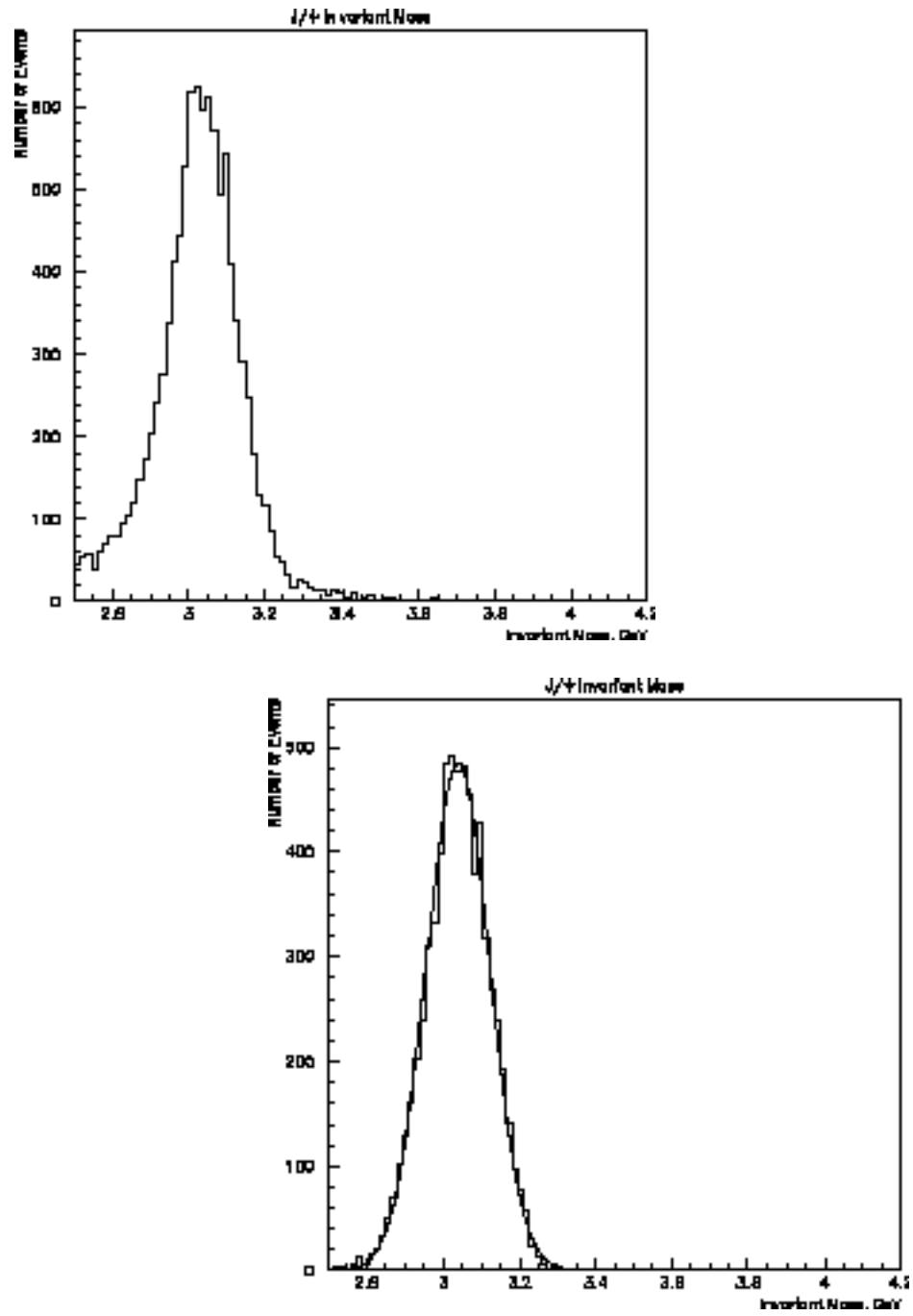distributions shown at the bottom of Figures 6.7 and 6.8 demonstrate the mass

resolution of the central calorimeter.

Figure 6.7: J/ψ Invariant Mass distributions before any analysis cuts (top) and after all other analysis cuts (bottom).
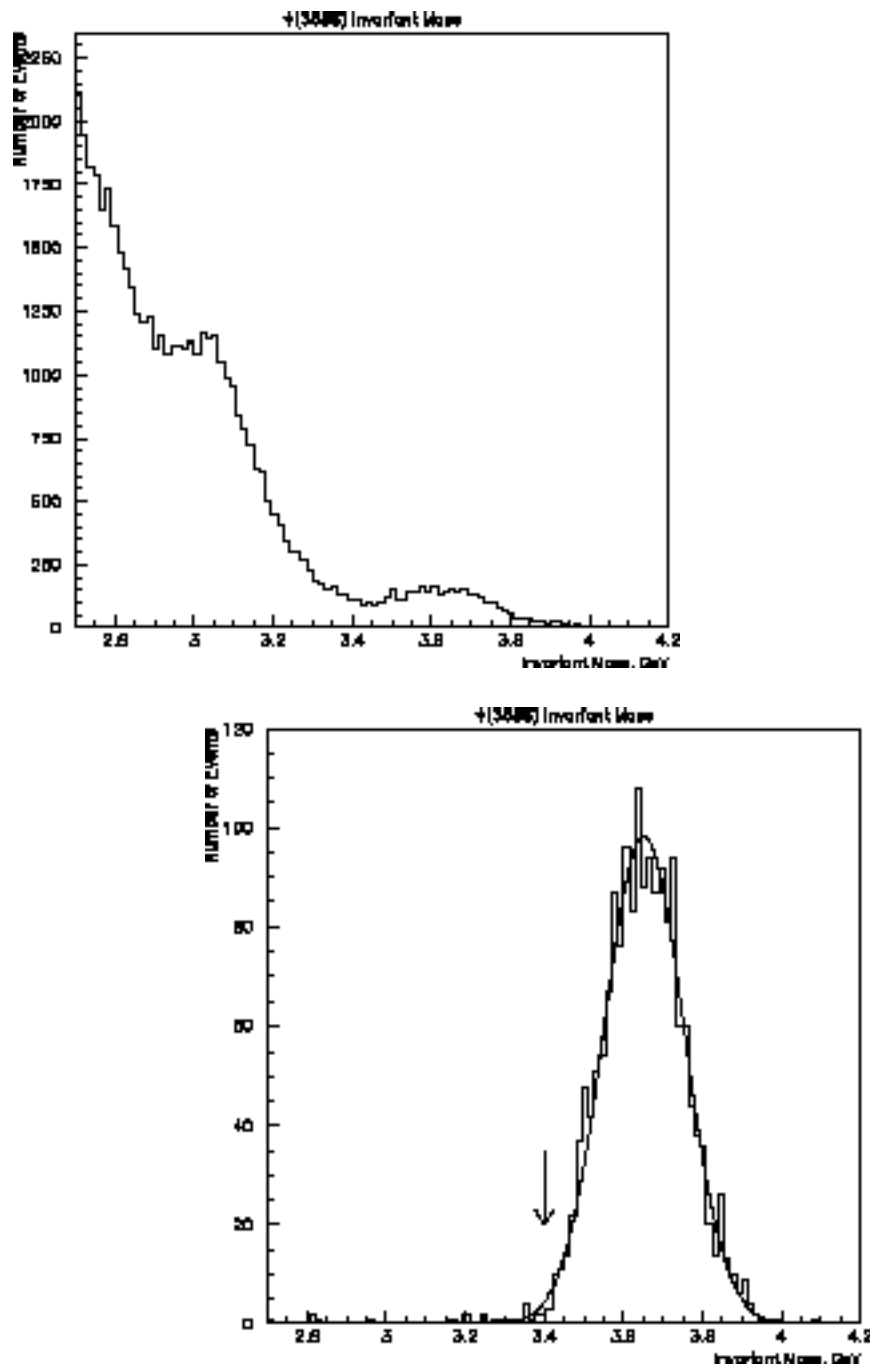
Figure 6.8:   (3686) Invariant Mass distributions before any cuts
                (top) and after all other cuts are applied (bottom).

Next, events are removed if their acoplanarity and akinematics are too large. These two quantities are evaluated using the CCAL polar angles instead of those given by the scintillating fibers, since CCAL cluster formation is the primary factor in selecting tracks. In the center-of-mass frame, the electrons from an exclusive charmonium decay should come out back-to-back. Zero acoplanarity means the event is exactly back-to-back in terms of the azimuthal angle. Zero akinematics means the event is perfectly back-to-back in terms of the center-of-mass polar angle. In practice, both quantities have a distribution centered on zero for pure e^+e^- events due to the resolution of the central calorimeter. If the acoplanarity or akinematics is greater than 25 milliradians, the event does not contribute to the angular distribution of either resonance's exclusive decay.

In Figures 6.9 and 6.10 are shown the acoplanarity and akinematics distributions for the J/ respectively (before any cuts and after all other cuts). The corresponding distributions are presented in Figure 6.11 and Figure 6.12 for the '. As seen previously in the invariant mass plots, the J/ sample is much cleaner than the ' sample to begin with, and the other cuts do a good job in cleaning up both decay channels.
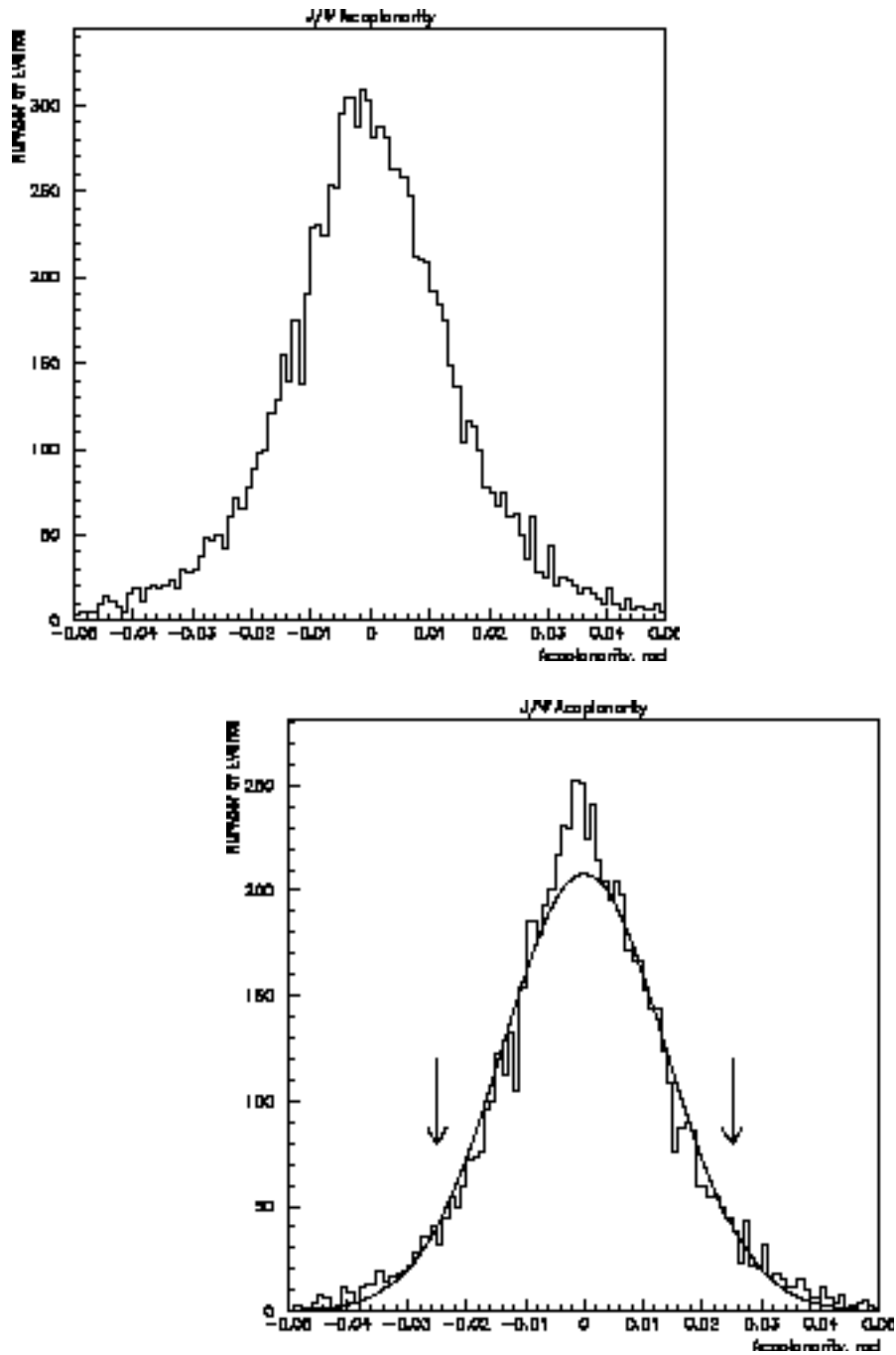
98

Figure 6.9: J/ψ Acoplanarity distributions before any cuts (top) and after all other cuts(bottom) are applied. Arrows represent the cut made on Acoplanarity.

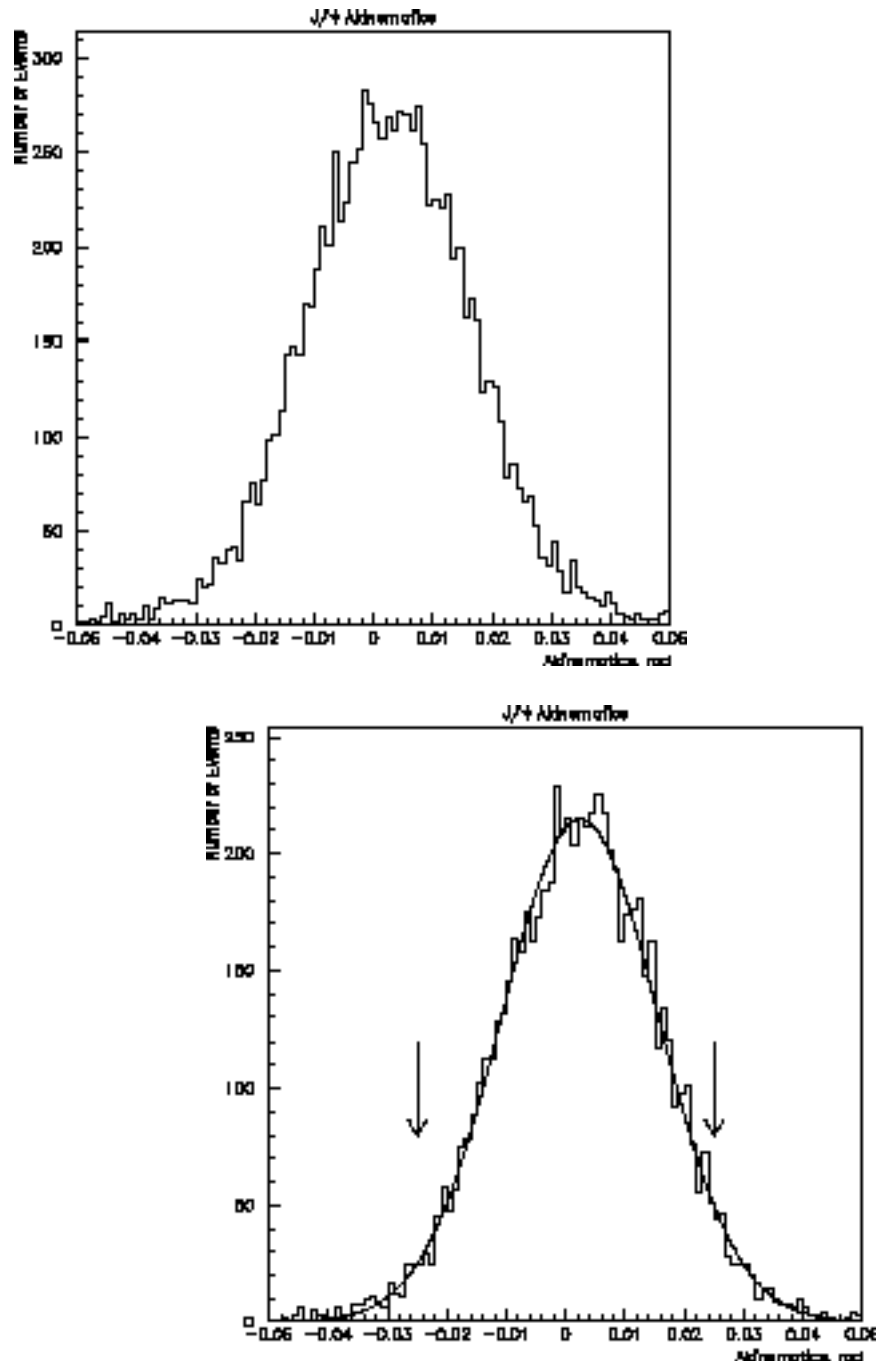Figure 6.10: J/ψ Akinematics distributions before any cuts (top) and after all other cuts (bottom) are applied. Arrows represent the cut made on Akinematics.
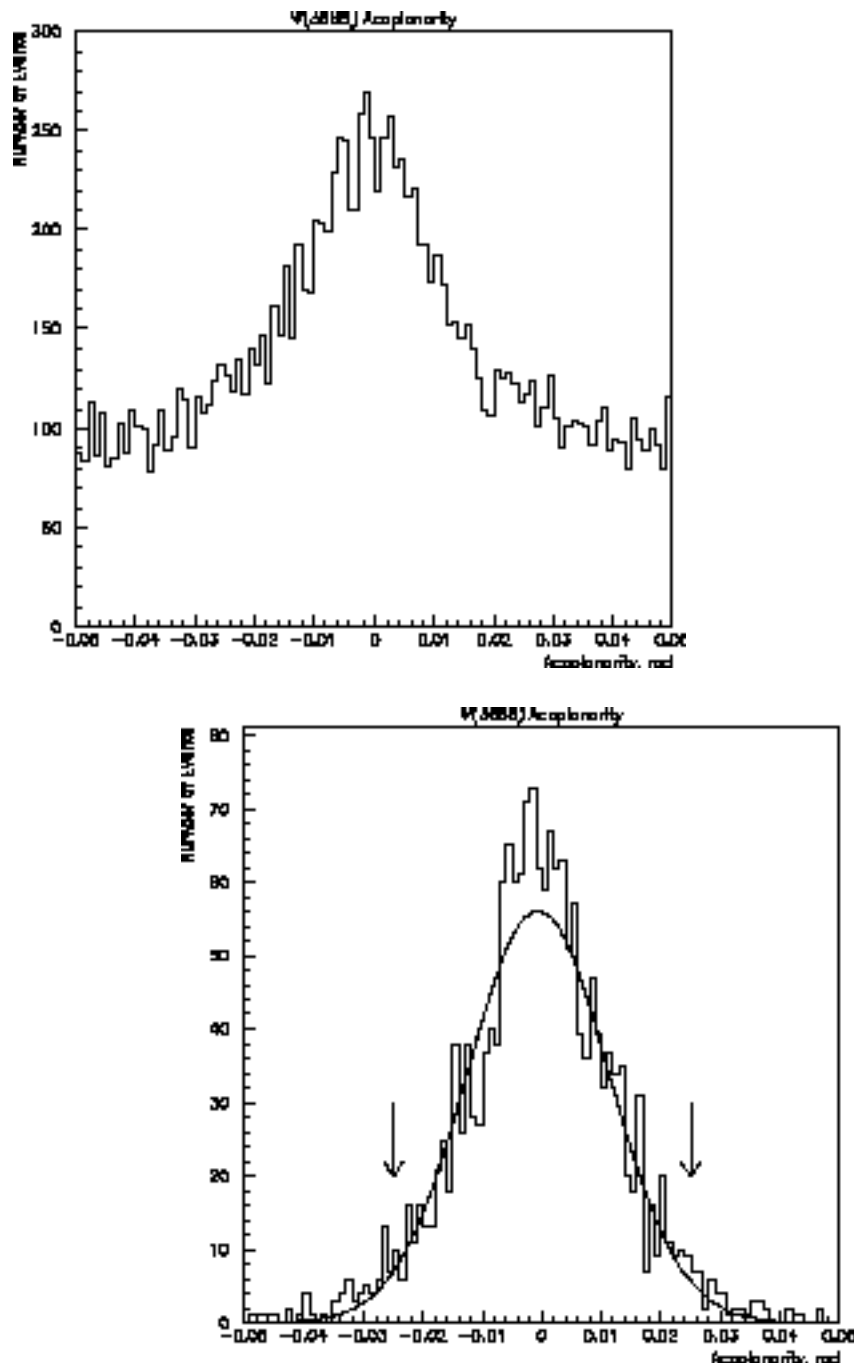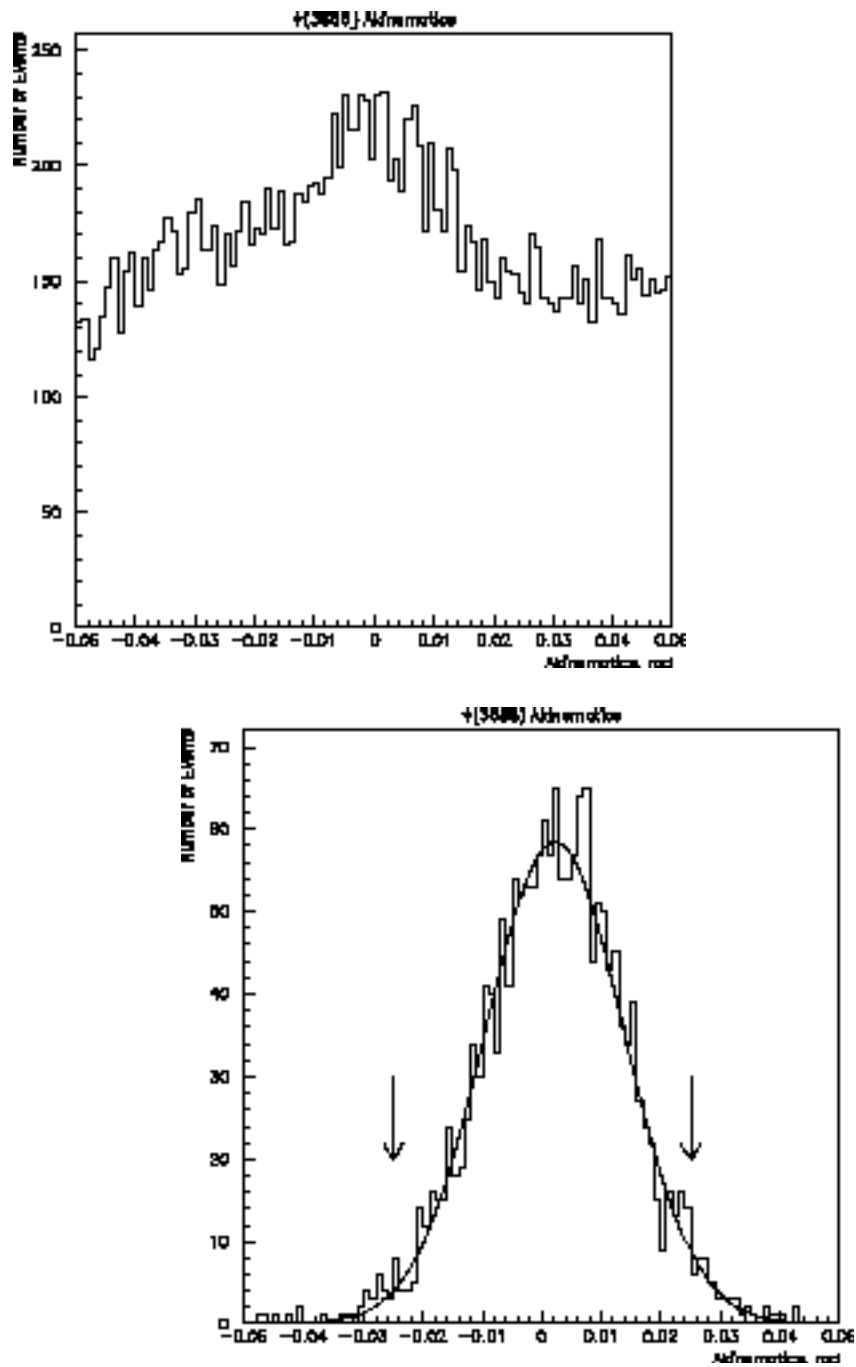
100

Figure 6.11: (3686) Acoplanarity distributions before any cuts (top), and after all other cuts (bottom) are applied. Arrows represent the cut made on Acoplanarity.

Figure 6.12:   (3686) Akinematics distributions before any cuts (top) and after all other cuts (bottom). Arrows represent the cut made on Akinematics.

Finally, a cut is made on the total energy of the e^+e^- pair. After all other

cuts in Table 6.2 have been applied, a Gaussian is fit to the bottom of Figures

6.13 for the J/   and 6.14 for the   '. Events that lie outside the mean total

energy +/- 2   are cut, which results in 4.71 GeV < ETOT < 5.31 GeV for Figure

6.13, and 6.72 GeV < ETOT < 7.62 GeV for Figure 6.14.

The end results of all these cuts are two very clean samples from which

to study exclusive decays of charmonium to e^+e^- pairs. Furthermore, to

underscore this point, the efficiencies of the various cuts in Appendices A and B

are consistent among the various data sets included.   But before presenting the

final angular distributions, we must first estimate how much of the background

was not excluded by the analysis cuts, and address the possibility of any bias in

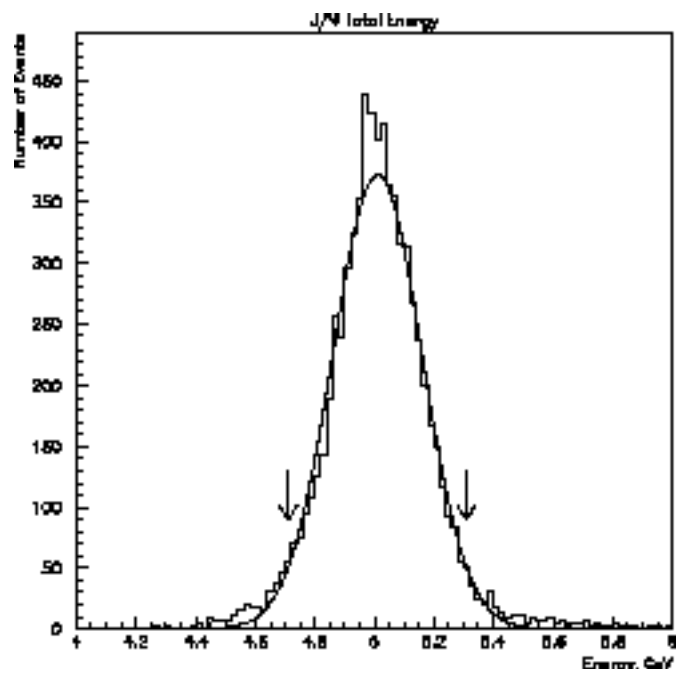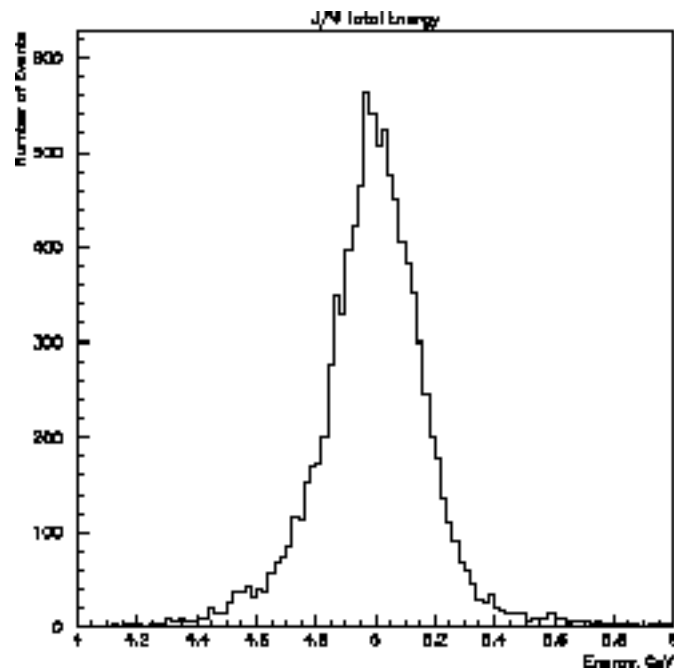the electron trigger (which is used to flag and write the data to tape).

Figure 6.13: J/ψ Total Energy distributions before any cuts (above), and after all other cuts (bottom) are applied. Arrows show where the Total Energy cut is made to the sample.
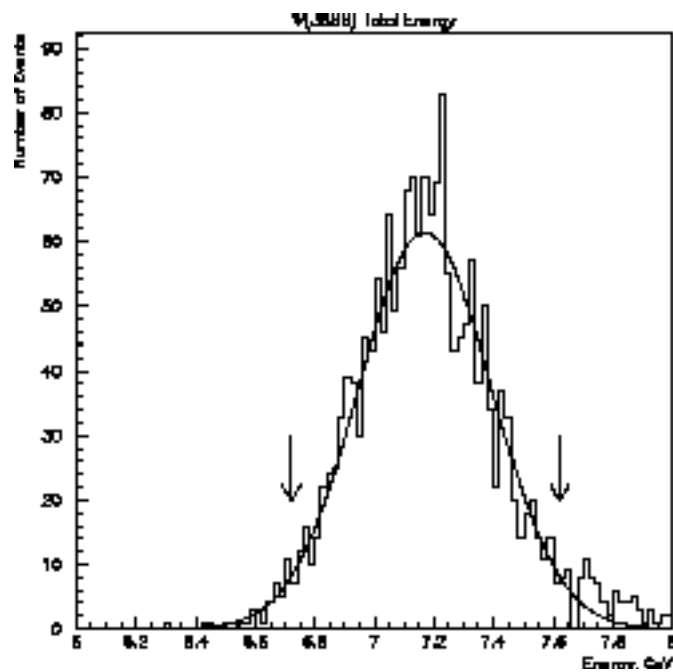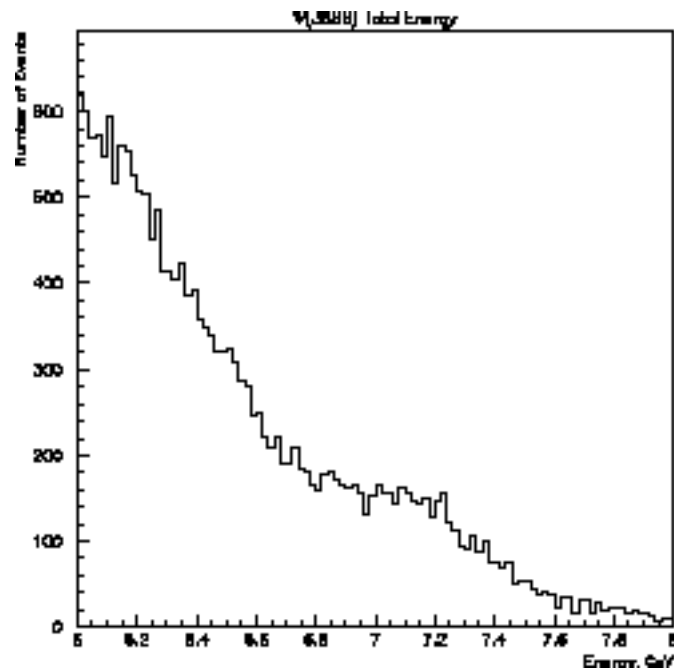
Figure 6.14:   (3686) Total Energy distribution before any cuts (top)
and after all other cuts (bottom) are applied. Arrows show where the
Total Energy cut is made to the sample.

6.4. Background to the Thesis Sample.

Despite having removed most of the background to these two exclusive decays, there is still a possibility that some contamination remains underneath the invariant mass distributions in Figures 6.7 and 6.8. The effect of this particular contribution is evaluated below.

Two different sets of runs used in the search of the η_c' (2^1S_0) are utilized here to determine the amount of background present in the data from the e^+e^- continuum or any remnant of the multi-pion decays: Runs 1283-1289 were taken at 3576 MeV, and runs 1180-1184 were taken at 3660 MeV. The quantum numbers of the η_c' do not permit it to decay directly to e^+e^-, and below the threshold for OZI-allowed decays only the J/ψ and the ψ' are allowed to do so.

Both sets of data went through the same analysis flow chart shown in Figure 6.1, with the centers-of-mass given as 3576 MeV and 3660 MeV respectively. Likewise the same cuts in Table 6.2 are applied; however the total energy cuts are a bit closer to the ψ' (6.5 GeV < ETOT < 7.6 GeV) and the invariant mass cut is 2.7 GeV for both background runs. The clusters representing the background candidates were a) on-time and b) had the

invariant mass closest to the center-of-mass. The results are compared to both

the J/ψ and the ψ'.

The invariant mass distributions of the background candidates are

presented in Figure 6.15 for the set at 3576 MeV and in Figure 6.16 for the set at

3660 MeV.   The rationale for cutting events with an invariant mass of less than

2.7 GeV can clearly be seen in both of these figures: The background without

any cuts increases rapidly below this threshold. After applying all the analysis

cuts, very few electron candidates remain, as one can see in Table 6.3, and the

bottom of Figures 6.15 and 6.16.

In order to evaluate the number of background candidates that may

contribute to the fit, the number of electrons actually falling within the fitting

region needs to be found. Figure 6.17 shows the angular distribution of

background candidates falling within the ψ' fitting region (which is larger in the

center-of-mass).   These distributions are created with respect to the CCAL
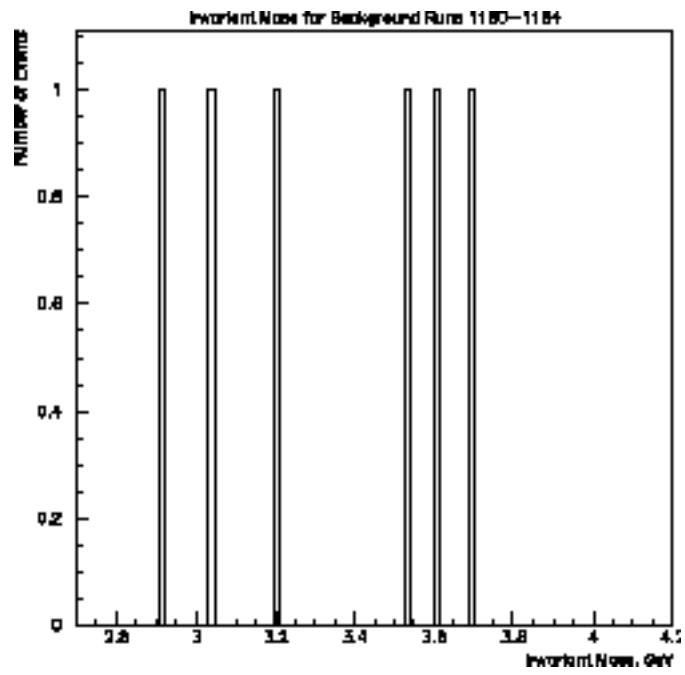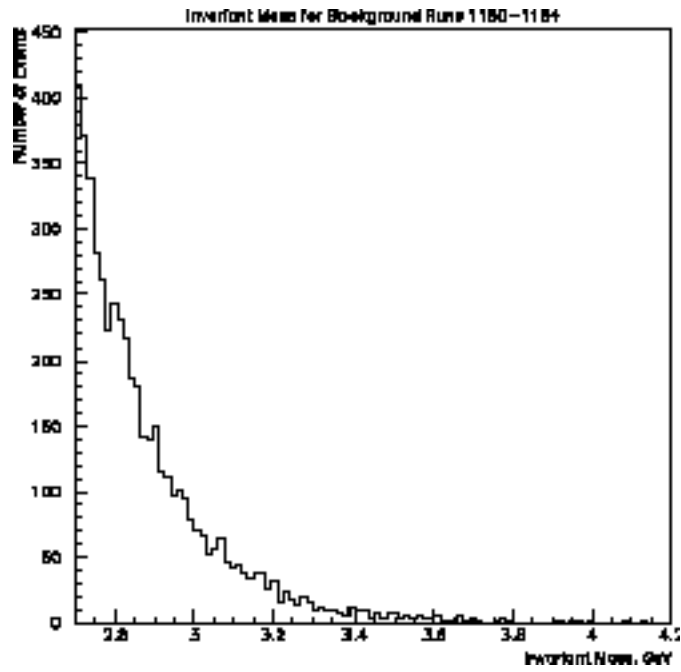
polar angle.

Figure 6.15: Invariant mass distributions for Runs 1180-1184 before any cuts are made (top) and after all cuts (bottom) are made.
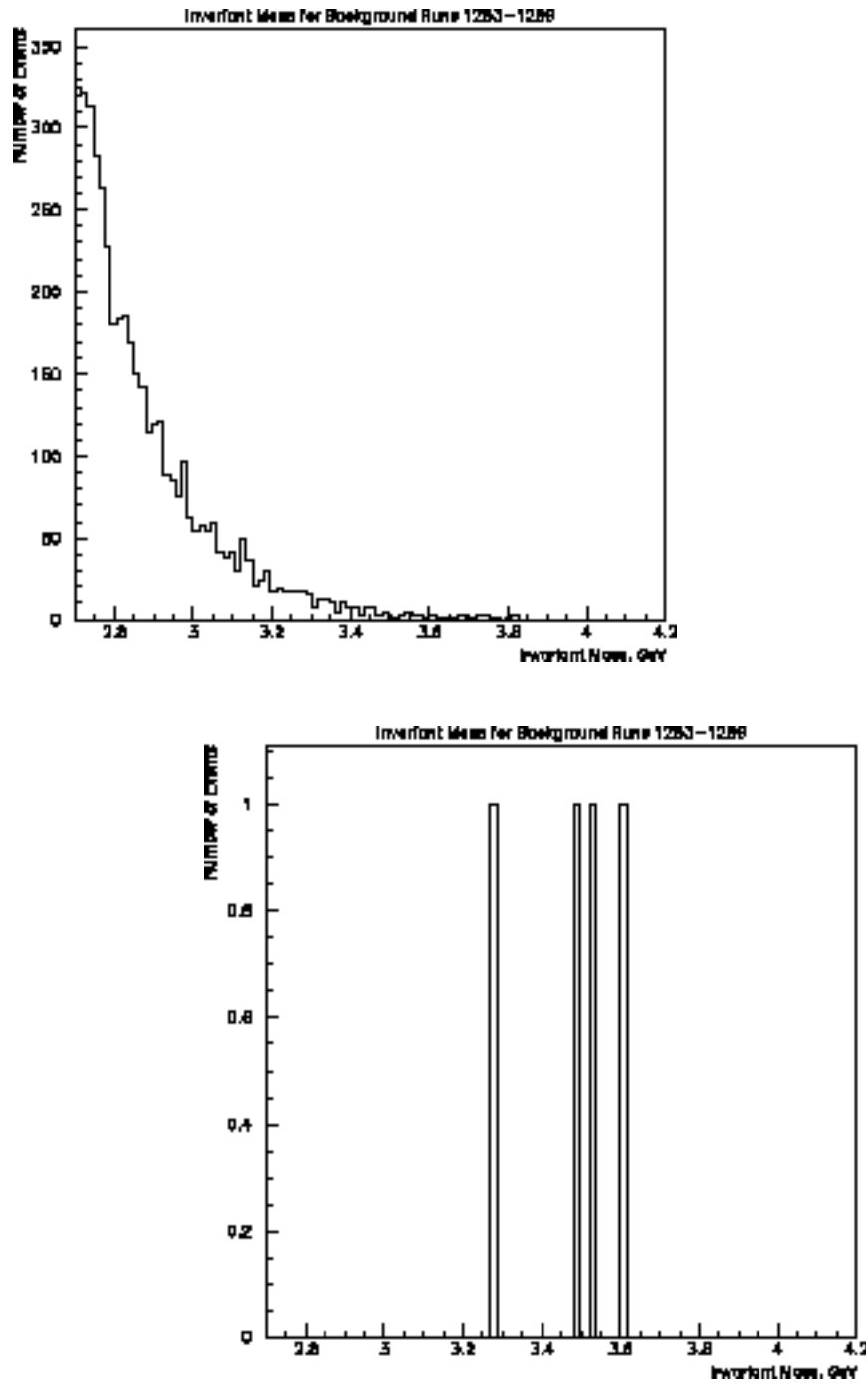
Figure 6.16: Invariant mass distributions for Runs 1283-1289
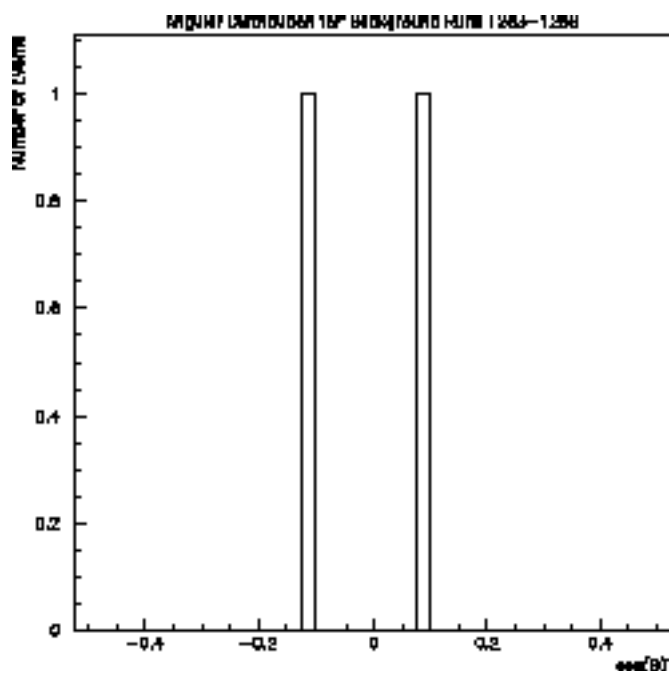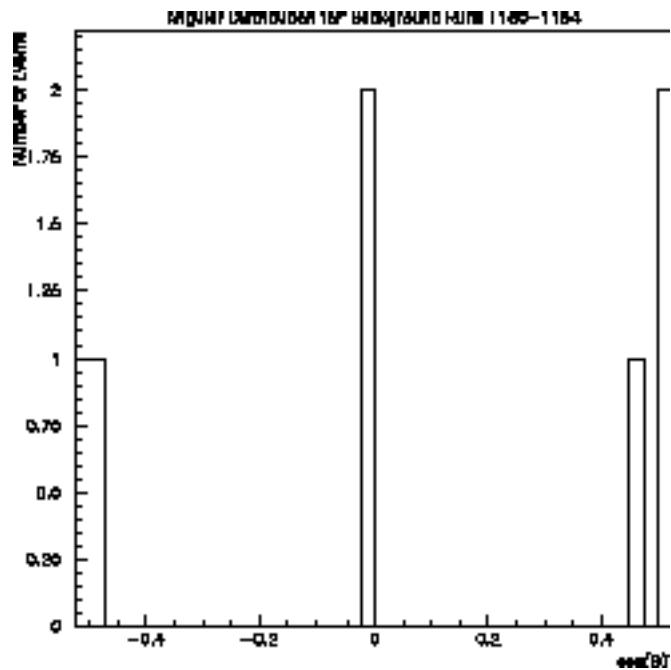before any cuts (top) and after all cuts (bottom) are made.

109

Figure 6.17: Angular Distributions for Background Candidates
passing all cuts for Runs 1180-1184 (top)
and Runs 1283-1289 (bottom).

110

Table 6.3 estimates the maximum amount of background contamination left underneath the invariant mass distributions assuming that the same percentage of background occurs for both resonances. An invariant mass cut of 3.4 GeV, the inefficiency of the fibers at large polar angles, and a smaller window in the center-of-mass will reduce these estimates. Taking the average of these two estimates predicts approximately 10 background events for the J/ (~0.1%), and about 50 background events for the   ' (~1.85%).

Background Sample	Invariant Mass	Number of electrons in n-tuple	Background electron candidates	Background candidates at J/ (19,540 in n-tuple)	Background candidates at ' (108,422 in n-tuple)
Runs 1283-1289	3576 MeV	8612	2	4.5	25.2
Runs 1180-1184	3660 MeV	9784	7	14.0	77.6

Table 6.3 : Background estimate from off-resonance data.

6.5. Dependence of the Electron Trigger on the Polar Angle.

One further source of inefficiency which could effect the shape of the angular distribution may come from a polar angle dependence of the electron trigger. The electron trigger (see Table 6.4) is made up of the following trigger requests: CMLU(1)*PBG3 + CMLU(2), where CMLU(1) is 2e*(H2<6) + 1e*2h(H2=2)*COPL , and CMLU(2) is 2e*(H2=2)*COPL*(Veto on FCH), and

PBG3 is the 1 to 3 back-to-back super-cluster requirement.

The efficiency of the charged trigger (CMLU(1)) was examined during a special trigger run in April of 1997,[94] in which data were taken by replacing the 2-electron trigger (2e) with a 1-electron trigger (1e) in order to determine the efficiency of detecting an electron. However, the statistics were too limited to conclude that there was any polar angle dependence. Such a dependence might arise if there were a degradation of the hodoscopes along the z-axis (perhaps a result of radiation damage near the interaction point), but this was not visible. Above and beyond the azimuthal inefficiency brought about by cracks between the elements of the H1 hodoscope, the data taken during this trigger run was consistent with having no azimuthal dependence either. Since the efficiency of the electron trigger is considered to be flat in the center of mass frame, it should not affect the shape of the angular distribution. As a result, the data is not corrected for any polar angle dependence of the electron trigger.

CMLU(1)	Output 1 of the Charged Memory Lookup Unit
CMLU(2)	Output 2 of the Charged Memory Lookup Unit
PBG1	Super-clusters of "electrons" are directly opposite each other.
PBG3	The other "electron" is in one of the 3 opposing super-clusters
1e	At least one Cerenkov cell has a charged track through it.
2e	At least two Cerenkov cells have charged tracks through them.
H2=2	Only 2 of the 32 H2 elements are hit.
H2<6	Less than 6 of the 32 H2 elements are hit.
COPL	2 H2 elements are coplanar.
FCH	More than one forward hodoscope is hit.

Table 6.4 : Definitions for the E835 e+e- trigger.